Hindawi
Geofluids
Volume 2022, Article ID 5815411, 14 pages
https://doi.org/10.1155/2022/5815411

*Research Article*

# Thick-Anchored Dual-Layer Locking Supporting Technique in Gob-Side Entry Driving with the Narrow Pillar: A Case Study

**Changliang Han**,[1] **Yuxin Yuan**,[1] **Nong Zhang**,[1,2] **Yi Zhao**,[3] **Qisheng Zhang**,[3] **Kai Song**,[4] **Min Wei**,[4] **and Yuxin Guo**[1]

[1]*State Key Laboratory of Coal Resources and Safe Mining, School of Mines, China University of Mining and Technology, Xuzhou, Jiangsu 221116, China*
[2]*School of Civil Engineering, Xuzhou University of Technology, Xuzhou, Jiangsu 21018, China*
[3]*Lanxian Zhengli Coal Industry, Shanxi Coking Coal Group Co., Ltd., Lvliang, Shanxi 033500, China*
[4]*Shandong Yanmei Heibao Mining Equipment Co., Ltd., Jining, Shandong 272000, China*

Correspondence should be addressed to Yuxin Yuan; yuanyuxin@cumt.edu.cn

Received 2 October 2022; Revised 10 December 2022; Accepted 13 December 2022; Published 21 December 2022

Academic Editor: Yu Wang



Roadway maintenance of the gob-side entry driving with narrow pillars is a key issue that needs to be considered in underground mining. In this paper, a thick-anchored dual-layer locking (TADL) supporting technique is proposed, in which, the flexible bolt and the cable are used as the main bodies of the foundation supporting layer and the deep reinforcement layer, respectively. In the instantaneous deformation stage after excavation, TADL is applied to form a thick-anchored bearing structure in time, aiming to achieve the following effects: (1) prevent the delamination of the roadway at the initial stage of excavation, (2) avoid the reduction of the bearing capacity of the surrounding rock structure, and (3) effectively control the plastic zone development and surrounding rock deformation of roof strata. Finally, the mining conditions of gob-side entry driving with narrow pillars are selected for engineering application and verification. The results of numerical simulation and field industrial tests show that the TADL support technique can effectively control the deformation of surrounding rock and drive away tensile stress. Compared with the original support scheme, the roof displacement of the roadway is significantly reduced by more than 16% after TADL support. This study provides a reference for the stability control of roadway roofs under similar conditions.

## 1. Introduction

The gob-side entry driving with narrow pillar (GSED-NP) is a roadway arrangement method to excavate the roadway along the edge of the goaf after the stabilisation of the strata movement in the gob [1–3]. In practical production, the gob-side entry is affected by two factors, i.e., the long-term slow pressurization effect of the abutment pressure formed by the transfer of the overlying strata load support point to the depth of the coal wall and the severe dynamic load resulting from the rotation subsidence of key rocks after the lateral roof fracture in goaf [4–6]. These issues can cause roof subsidence and coal pillar instability in gob-side entry, which brings great trouble to mine production. Therefore, stability control of the surrounding rock in the GSED-NP has become the key to achieving high production and high efficiency in mines.

Many scholars have researched the surrounding rock deformation and control technique of GSED-NP. Existing studies worldwide mainly focus on the redistribution of surrounding rock stress caused by mining, the formation of overlying rock structures on the load size of gob-side roadway, and the influence of coal pillars on surrounding rock deformation. For example, the lateral-bearing pressure along the coal body edge can be divided into a relaxation area less than the original rock stress, a bearing pressure area with high-concentrated stress distribution, and an original rock stress area [7], which has become a consensus in the academic community. Hou and Li [8], Qian et al. [9], and Xingzhu et al. [10] studied the influence of the mechanical structure formed after the gob roof was broken on

the gob-side roadway and analyzed the deformation and load size change of the roadway caused by the rotary subsidence of the arc triangle key block. Shiliang [11] proposed the influence pattern of the coal pillar width on the support pressure distribution in pillarless mining. Nhong et al. [12], Changliang et al. [13], and Yuan et al. [4] studied the influence of the gob-side roadway by the slow subsidence of the hard roof on the gob-side and the intense pressure and proposed a flexible anchor support system based on the support concepts of "trans-boundary" and "thick-anchored".

The bolt-cable combined support is mainly used for supporting structure reinforcement to control the deformation under strong mining conditions. In recent years, many researchers have established a bolt-cable supporting system for strong mining conditions by improving the basic structure of the bolt-cable. For example, Wang et al. and He et al. [14, 15] proposed a constant-resistance and large-deformation anchor cable suitable for GSED-NP. When the cable reaches the designed resistance, the resistance remains constant with the increase of the surrounding rock deformation. In this way, space is provided for the release of elastic strain energy, and the occurrence of strong mineral pressure is avoided to some extent. Yuan et al. [4] designed a new type of flexible bolt that breaks through the space limitations of traditional rigid bolts. Wang et al. [16–18] arranged the cable in the deep stable rock formation, so as to mobilize a wider range of rock mass to restrain deformation, which makes full use of the bearing performance of the surrounding rock. They all believe that bolt-cable support aims to give full play to the bearing performance of the rock mass.

This paper proposes a thick-anchored dual-layer locking supporting technique to solve the surrounding rock control problem of the GSED-NP. The mining conditions of GSED-NP are selected for engineering application and verification.

## 2. Case Study

*2.1. Description of the Mining and Geological Conditions.* Lanxian Zhengli Coal Industry is located in Shanxi province, China, with a coal production capacity of 1.5 million tons/year. Its 4-1 coal seam has a buried depth of 490 m and a thickness of 2.87-3.64 m. The immediate roof is siltstone interbedded, and the main roof is mainly medium fine sandstone. The lithologic characteristics of the roof are shown in Table 1. Currently, the first mining area of this seam is being mined, with seven working faces arranged in the south wing, and skip mining takes over between sections. Because the mine pressure was not avoided, the gob-side entry was severely deformed, which needs to be renovated several times. As a result, the working face $14^{-1}$105 is about to face a strong mining challenge in the island working face.

The research object, headentry of $14^{-1}$105, which is located on the east side of the working face $14^{-1}$106, is a rectangular section. It is excavated along the mine-out $14^{-1}$104 and the 4-1 coal floor, with a net section of 4.6 m × 3.2 m, and a total length of the roadway of 566 m. The pillar widths of the working faces $14^{-1}$105 and $14^{-1}$104 sections are 6 m. The mining layout is shown in Figure 1.

Table 1: Lithology of the study site.

| Lithology | Thickness (m) | Depth (m) | Remarks |
|---|---|---|---|
| Sandstone | 50 | 416 | Overlying strata |
| Sandy mudstone | 31 | 447 | Key stratum |
| Siltstone | 11 | 458 | Overlying strata |
| Fine sandstone | 14 | 472 | Key stratum |
| Siltstone | 8 | 480 | Main roof |
| Sandy mudstone | 6.8 | 486.8 | Immediate roof |
| $4^{-1}$ coal | 3.2 | 490.0 | Coal |
| Fine sandstone | 6 | 496.0 | Immediate floor |
| Sandstone | 20 | 516.0 | Main floor |

*2.2. Original Supporting Scheme and Failure Description.* Damage characteristics of the headentry of $14^{-1}$106 gob-side entry are shown in Figure 2, and the original supporting scheme adopts a left-handed-threaded steel anchor rod without longitudinal reinforcement with cable support. Six pieces of $\Phi 20 \times 2200$ mm-threaded steel bolts are arranged in each row of the roadway roof, with the row spacing of 800 × 1000 mm; two or three $\Phi 18.96 \times 6500$ mm cables are arranged every two rows of cables, forming a "3-2" arrangement. Four $\Phi 20 \times 2200$ mm-threaded steel bolts are arranged in each row of the side wall, with a row spacing of 1000 mm, and the spacing is different. The pretightening torque of the threaded steel bolt shall not be less than 60 kN, and the preload of the cable shall not be less than 300 kN.

Figure 2(b) shows the original supporting scheme in $14^{-1}$106 headentry. As shown in the figure, the roof surface is severely fractured; the rocks fall in the shape of nets; the passive supporting members (channel steel and steel tape) mostly extrude in the middle of the roadway; and the edge of the tray is raised. The above-mentioned phenomenon indicates that uneven deformation exists in the rock stratum, i.e., delamination at a certain horizon from the roof. It shows that the surrounding rock is deformed unevenly, and the deep rock layer may have an arched structure after breaking.

## 3. Thick-Anchored Dual-Layer Locking Supporting Technique

As shown in Figure 3, the surrounding rock is distributed in the sequence of excavation damaged zone, excavation-influenced zone, and intact zone (Renaud et al. [19] and Wang et al. [16]) after the excavation of the roadway. According to the research in the literature (Wang et al. [16]), an excavation damaged zone is an annular fracture zone generated under strong mining disturbance during roadway excavation and mining. In this area, the rock structure is severely damaged, and the strength of the rock mass is between the peak strength and the residual strength (Figure 3). Without external constraints, the bearing capacity will lose completely, and thus, the excavation damaged zone is the main control object in the supporting system. Excavation-influenced zone refers to the surrounding rock with lower stress than the peak strength, less fissure development, and a complete rock mass structure. The intact zone refers to the surrounding rock whose stress is equal to the in situ

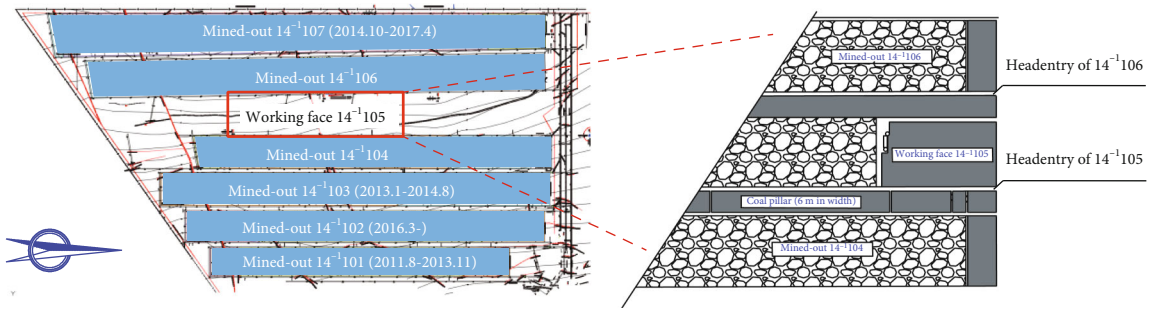


Figure 1: Mine location and panel layout of the test areas.

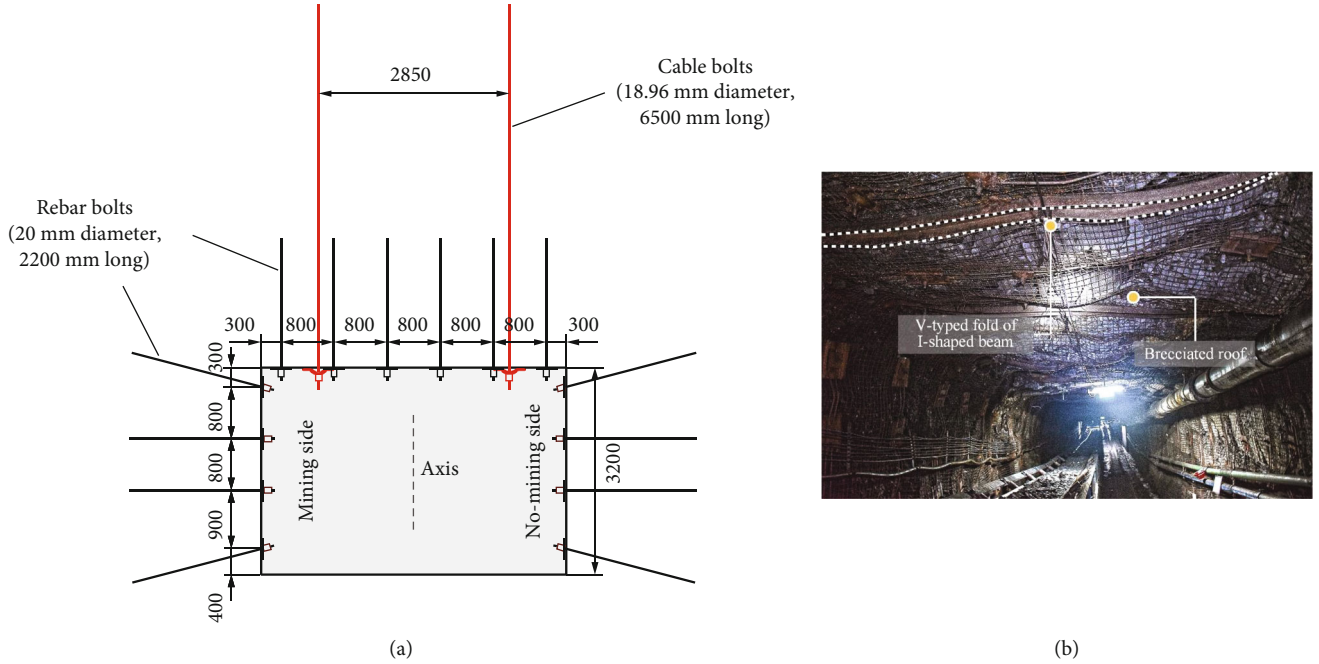


Figure 2: (a) Original support scheme. (b) Damage characteristics of the headentry of 14⁻¹106.

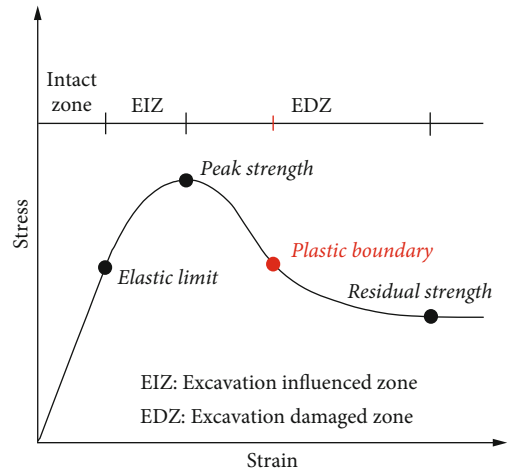


Figure 3: Locations of excavation-influenced zone, excavation damaged zone, and plastic boundary in the stress-strain curve (modified from Renaud et al. [19] and Wang et al. [16]).

stress and is not affected by mining disturbances. Suppose the anchorage end is arranged in the excavation-influenced zone, the self-supporting performance of the rock mass in this area and deeper places can be fully mobilized, and the deep-shallow linkage can be realized. Therefore, the rock mass in this area can be used as the bearing body of the supporting system.

In the case of narrow pillar in the gob-side entry driving, the coal series-layered roof is mostly compressed and bent under the action of bending moment. The mechanical model of fixed support at one end and hinged support at the other is established, as shown in Figure 4.

According to the maximum tensile stress theory (the first strength theory), after the bending deformation of the roof rock beam, the most dangerous point of the roof rock beam is the failure of the tensile stress in the middle. The bending moment in this section is

$$M = \frac{ql^2}{8}, \quad l = w + w_1 + w_2. \tag{1}$$

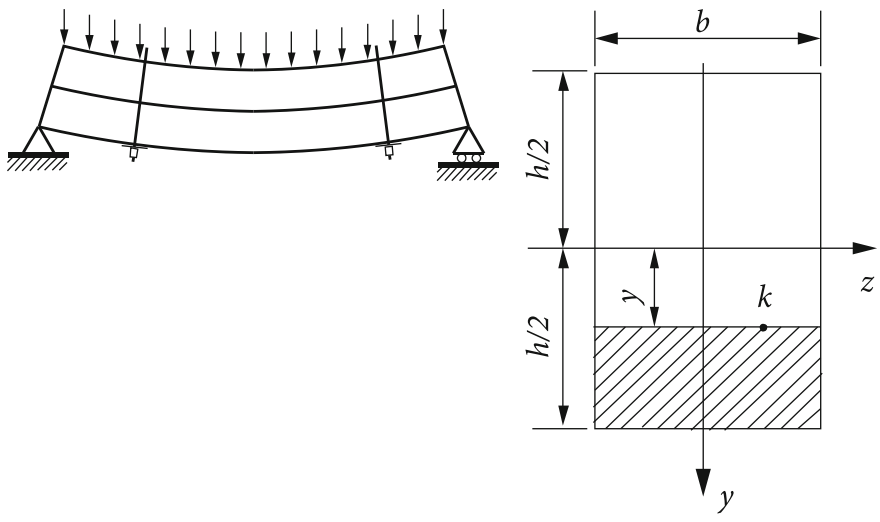


Figure 4: Schematic diagram of the shear force carried by the anchor when the rock beam bends. (a) With anchor. (b) Shear stress at any point $k$ on the cross-section at a distance $y$ from the neutral axis during rock bending.

Thus, the maximum tensile stress can be obtained

$$\sigma \frac{My}{I_z}. \tag{2}$$

And because

$$I_Z = \frac{bh^3}{12}. \tag{3}$$

Thus, the maximum tensile stress

$$\sigma = \frac{12My}{bh^3}. \tag{4}$$

And when $y = h$, the tensile stress takes the maximum value

$$\sigma_{\max} = \frac{12M}{bh^2} \propto \frac{1}{h^2}, \tag{5}$$

Where $b$ is the cross-sectional width, which is taken as 1 according to the plane strain assumption; $h$ is the cross-sectional height; $M$ is the bending moment in the middle of the roof rock beam; $y$ is the distance from any point $K$ of the cross-section to the neutral plane; $w$ is the roadway width, taken as 5 m; $w_1$ is the loss caused by small coal pillar, taken as 1 m; $w_2$ is the loss value of solid coal side, taken as 1.5 m; $q$ is the load concentration, i.e., the dead weight load of the immediate roof; and $\gamma$ is taken as 27000 $N{\cdot}m^{-3}$. According to the stress concentration factor of 1.8, it is taken as 298.6 $kN{\cdot}m^{-1}$.

The value of $M$ is then obtained by substituting the above values into Equations (1)–(4). Therefore, the relationship between the maximum tensile stress of the roof $\sigma_{\max}$ and roof thickness $h$ is shown in Figure 5.

And it can be seen that the further from the surface, the smaller the tensile stress inside the roof rock. At a shallow depth of 4 m, the tensile stress inside the roof can reach 2 MPa, which is the primary factor of damage to the shallow surrounding rock. And when the depth beyond 4 m, the tensile stress decreases sharply and basically does not cause damage. In summary, it can be seen that the shallow range of 4 m is the critical range for applying prestressing support. The implementation of high-strength prestressing support in this area can realize the role of tensile stress driven and fundamentally solve the problem of tensile stress concentration in shallow surrounding rock. We can define this range as the critical anchorage thickness.

According to the above analysis, the TADL supporting technique is proposed (as shown in Figure 6), in which, the flexible bolt (as shown in Figure 7) is used as the main body of the foundation supporting layer, and the cable is used as the main body of the deep reinforcement layer. In the instantaneous deformation stage after excavation, the technique is applied to form a thick-anchored bearing structure in time to prevent the delamination of the roadway at the initial stage of excavation. In addition, it will prevent the bearing capacity of the surrounding rock structure from diminishing, thus timely and effectively restricting the plastic zone expansion and surrounding rock deformation of roof strata. The comparison of the performance parameters of this technique and the traditional bolt is shown in Table 2.

Constrained by the roadway's height and insufficient length, the rigid support cannot be bent, and thus the anchoring layer of sufficient thickness cannot be formed, resulting in the weak deformation resistance of the top plate. At the same time, the strength of the flexible steel strand is generally 1860 MPa, and the rigid bolt is generally 335~500 MPa. After the strength is increased, the locking ability is stronger.

The flexible bolt is composed of steel strand rod, locking sleeve, nut, spacer, arch tray, and antitorsional steel plate,

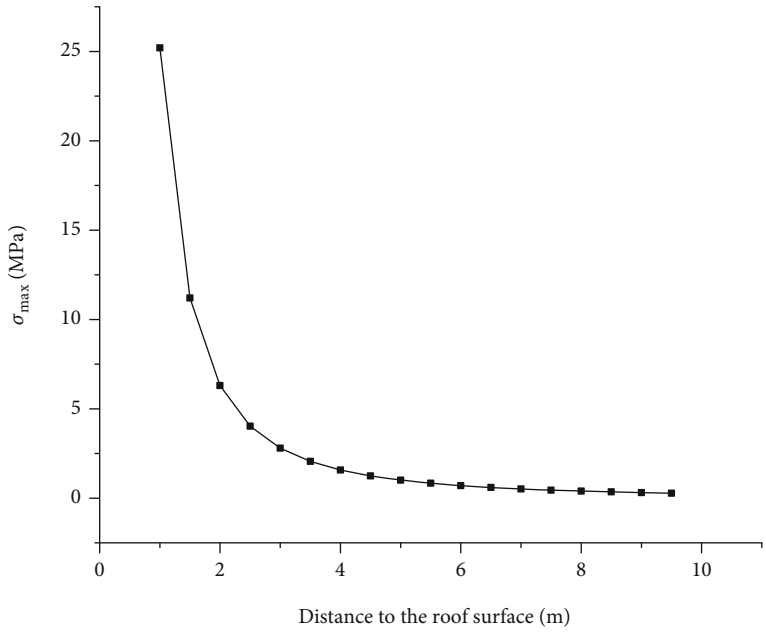


Figure 5: Tensile stress curve at different positions.

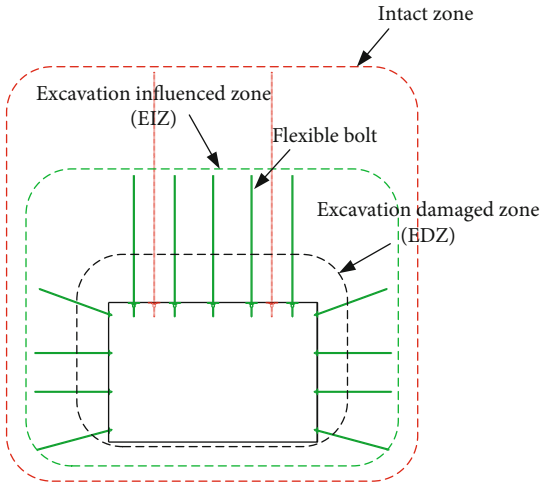


Figure 6: TADL supporting technology.

among which, the steel strand rod is composed of 19 strands of intertwined steel wires. The locking sleeve is fixed at the end of the stranded rod through the extrusion process and the wire rolling process, relying on the friction between the locking sleeve and the rod body so that it does not slip off and destroy. The length of the rod can be determined according to the needs of the project site. Since the rod is made of flexible material, the flexible bolt breaks through the limits of the height of the roadway and can be anchored to the deep and relatively stable rock layer.

## 4. Determination of Support Design by Numerical Simulation

*4.1. Numerical Model Establishment.* As shown in Figure 8, the model has a length of 700 m, a width of 200 m, and a height of 150 m. It assumes the retreat mining of $14^{-1}104$ and $14^{-1}106$ and entry development and retreat mining of $14^{-1}105$. In this paper, the Mohr-Coulomb criterion is adopted. The horizontal displacement at the sides and vertical movement at the base are limited, with a stress boundary at the upper surface. 9.1 MPa is used to simulate the self-weight of the overlying rock, and the lateral stress factor is 1.2. The minimum dimensions of the roadway cell are 0.2 × 0.2 × 0.2 m. The width of the coal pillar is 6 m. The physical and mechanical properties of the rock mass are shown in Table 3. Displacement and stress measurement stations are set up to monitor the roof deformation during the operation.

The numerical analysis is conducted in the following steps: (1) implement and initialize the in situ stress field; (2) extract working face $14^{-1}104$ in retreat at an interval of 20 m in the mining direction for each cycle until the entire working face is mined out; (3) extract working face $14^{-1}106$ as the same procedure; (4) excavate the headentry along its strike and apply support schemes (unsupported scheme, original support scheme, and the TADL supporting scheme), respectively; (5) step to solution and calibrate the deformation properties if needed; and (6) extract working face $14^{-1}105$.

*4.2. Simulation and Determination of Supporting Scheme.* The deformation of surrounding rock under different pillar widths is compared between the original supporting and the thick-anchored dual-layer locking supporting technique.

*4.2.1. Supporting Scheme.* Figure 9 shows that the optimal supporting scheme is the TADL supporting. Five $\Phi 21.8 \times 4300$ mm flexible bolts are arranged in each row of the roof, with the spacing of the bolt and row all being 950 mm × 1000 mm; in every two rows, flexible bolts are supplemented with two $\Phi 21.8 \times 6300$ mm cables, with the row and cable spacing of 2850 mm × 2000 mm; and four $\Phi 22 \times 2600$ mm

(a) (b)

Figure 7: Flexible bolts. (a) Type I in which pretightening force is applied through the lockset. (b) Type II in which pretightening force is applied through the nut.

Table 2: Comparison of bolt performance parameters commonly used.

| Parameters | Diameter (mm) | Length (m) | Yield strength (MPa) | Tensile capability (kN) | Elongation (%) | Pretension (kN) |
|---|---|---|---|---|---|---|
| Rebar bolts | 22 | 2.2~2.5 | 500 | 240 | 20 | ≤60 |
| Flexible bolts | 21.8 | 3.5~4.3 | 1600 | 560 | 7 | 250~300 |

left-handed-threaded steel bolts are arranged in each row of the side wall, with different bolt spacings and the row spacing of 1000 mm. The preload of the flexible bolt is not less than 200 kN, and that of the cable is not less than 300 kN.

*4.2.2. Simulation Results.* Figure 10 shows the vertical stress distribution of the surrounding rock under three roof-supporting schemes, i.e., unsupported, original support, and TADL support, of the headentry of $14^{-1}105$ when the pillar width is 6 m. As can be seen, a tensile stress concentration area exists in the unsupported roof, with the vertical surrounding rock stress. $\sigma_{zz}$ being less than 0.032 MPa. In this case, most of the superficial surrounding rock is in the tensile stress concentration area (as shown in Figure 10(a)). The vertical surrounding stress $\sigma_{zz}$ under the original support scheme and the TADL support are 0.11 MPa and 0.16 MPa, respectively. The above calculation results show that the TADL support can drive away the tensile stress. Considering that the tensile strength of coal measure sedimentary strata is much smaller than the compressive strength, the application of high-preload active support in the initial stage of stress release after roadway excavation can avoid the initial tensile deformation and separation of the roof rock mass.

Figure 11 shows the vertical displacement field and deformation curve of the roof of the headentry of $14^{-1}105$ under the three supporting schemes. It can be seen from Figure 12 that when there is no support, the displacement of the roof rock mass still does not converge when calculating 37000 steps. When the original and TADL support are used, the maximum displacement is 0.058 m and 0.050 m, respectively. After adopting TADL support, the roof displacement of the roadway is significantly reduced by more than 16%. The above results show that TADL support can effectively control the deformation of surrounding rock.

Compared with unsupported and original support, TADL support can improve the stress field of surrounding rock support and optimize the roof displacement to a certain extent. Therefore, in order to further verify the TADL support technique, the headentry of $14^{-1}105$ was supported by the support scheme shown in Figure 9 for further field applications.

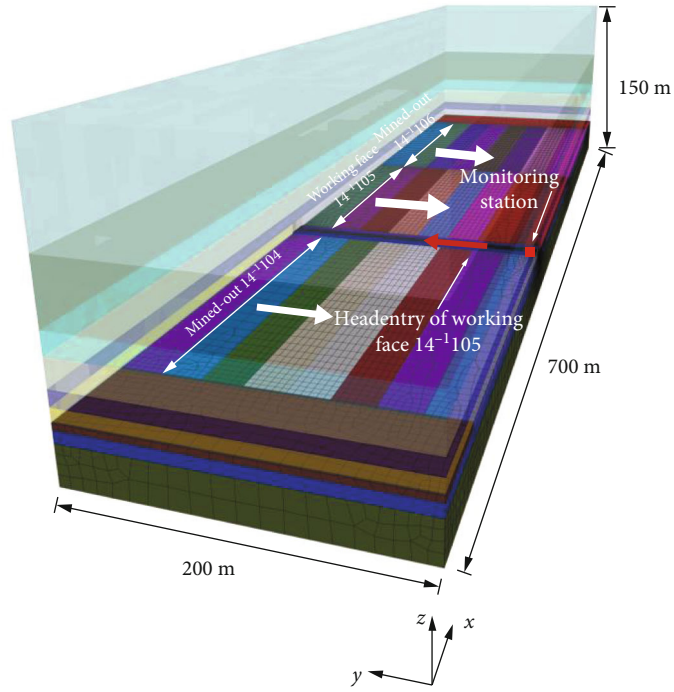


Figure 8: Sketch of the FLAC$^{3D}$ mesh for the working face 14$^{-1}$105.

Table 3: Rock strata properties used in the numerical model.

| Rock strata | Thickness (m) | Properties of rock mass | | | | | |
|---|---|---|---|---|---|---|---|
| | | Density (kg/m$^3$) | Cohesion (MPa) | Friction angle (°) | Tensile strength (MPa) | Bulk modulus (GPa) | Shear modulus (GPa) |
| Sandstone | 50 | 2264 | 3.62 | 38 | 1.24 | 5.43 | 4.15 |
| Sandy mudstone | 31 | 2395 | 2.87 | 36 | 1.78 | 6.42 | 5.76 |
| Siltstone | 11 | 2589 | 3.95 | 32 | 2.79 | 6.87 | 3.97 |
| Fine sandstone | 14 | 2564 | 2.81 | 38 | 1.65 | 7.42 | 2.15 |
| Siltstone | 8 | 2489 | 3.94 | 32 | 2.87 | 9.4 | 3.4 |
| Sandy mudstone | 6.8 | 2301 | 3.79 | 38 | 2.13 | 5.42 | 2.15 |
| Coal seam | 3.2 | 1421 | 1.41 | 31 | 0.97 | 2.43 | 1.8 |
| Fine sandstone | 6 | 2489 | 1.65 | 32 | 1.45 | 4.2 | 1.97 |
| Sandstone | 20 | 2264 | 3.8 | 38 | 1.96 | 2.42 | 2.15 |

## 5. Verification of Engineering Project

Five measuring points were arranged along the working face of 14$^{-1}$105 to carry out on-site monitoring of the roadway surface displacement, as shown in Figure 13.

(1) The analysis of the deformation characteristics of station 1 is shown in Figure 14(a). After excavating the roadway space, the roof subsidence undergoes a severe deformation phase within the range of 0~6 m (0~8 d) at a speed between 8 and 9 mm/d. In the range of 46~102 m (9~17 d), the slow deformation phase takes place at a deformation speed of 8~9 mm/d. 102 m (18 d) after excavation, the stable deformation phase occurs at a rate of 0~1 mm/d. The subsidence from these three phases accounts for 39.3%, 32.1%, and 28.6% of the total, respectively. The maximum subsidence speed of the roof is 12 mm/d, and the total subsidence after the deformation stabilized is 28 mm

(2) The analysis of the deformation characteristics of station 2 is shown in Figure 14(b). After excavating the roadway space, the roof subsidence is in a severe deformation phase within the range of 0~57 m (0~10 d), and the deformation speed at this stage is

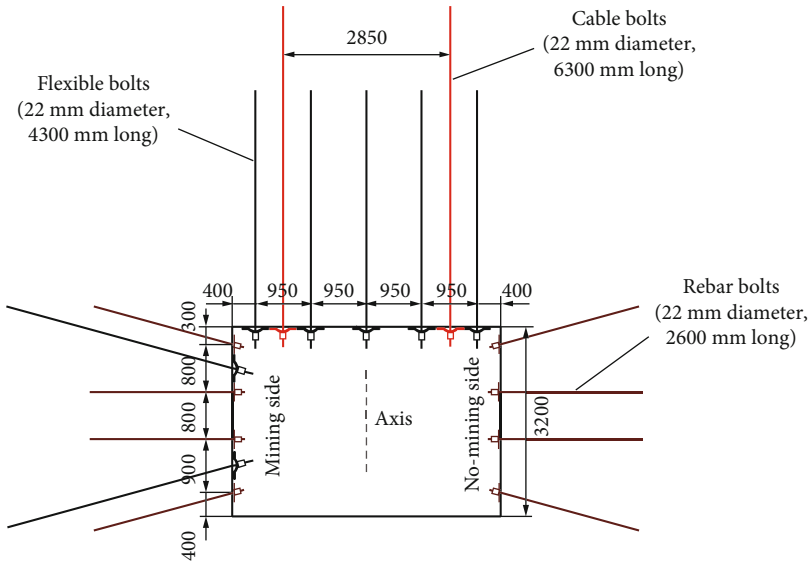


Figure 9: TADL supporting scheme.

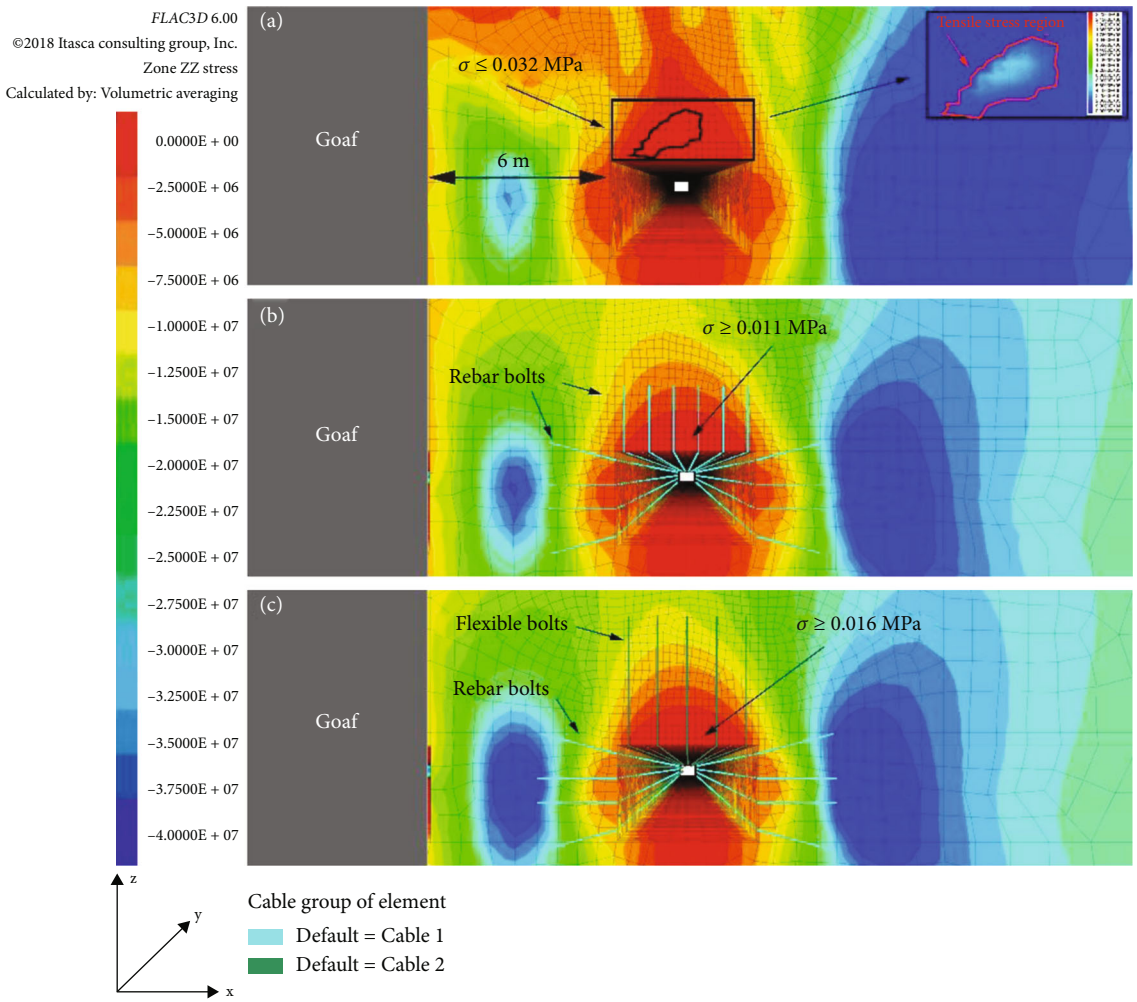


Figure 10: Comparison of vertical stress of roadway under (a) unsupported, (b) original support scheme, and (c) TADL support scheme.

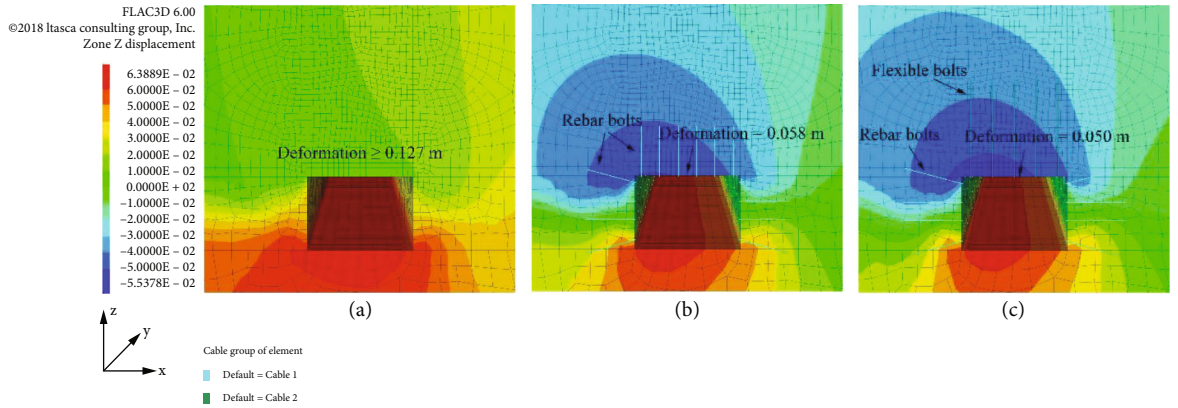


Figure 11: Comparison of vertical deformation of roadway under (a) unsupported, (b) original support scheme, and (c) TADL support scheme.

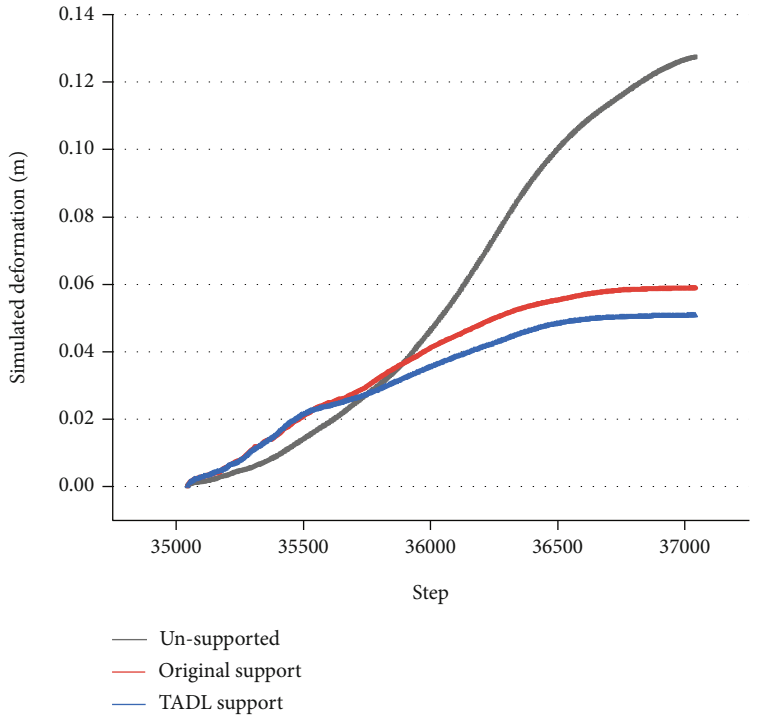


Figure 12: Simulated deformation curves of roadway under three support schemes. 0020.

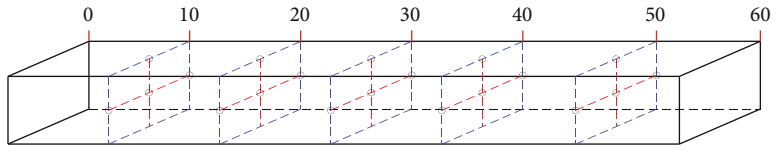


Figure 13: Monitoring scheme.

10 mm/d. The deformation slowed down in the range of 57~106 m (11~18 d), and the deformation speed decreased from about 10 mm/d to about 2 mm/d. 106 m (19 d) after excavation entered the stable deformation phase, and the deformation speed remained at 0~1 mm/d. The subsidence from these three phases accounts for 46.7%, 26.7%, and 26.7% of the total, respectively. The maximum subsidence speed of the roof was 11 mm/d, and the total subsidence amount after the deformation stabilized was 15 mm

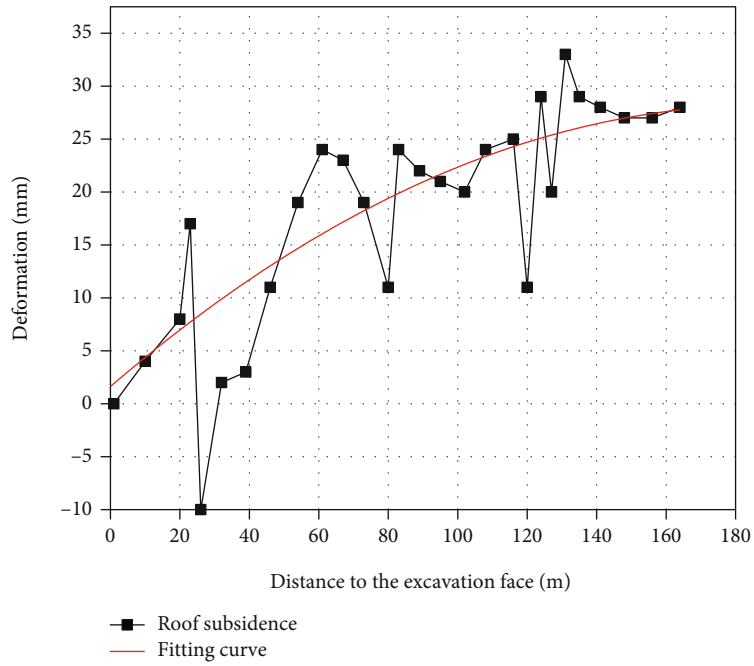


(a)

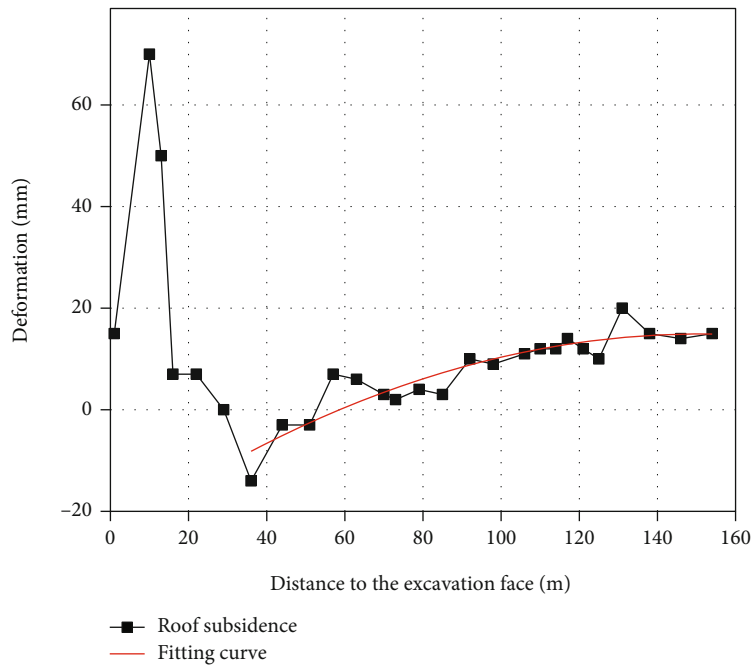


(b)

Figure 14: Continued.

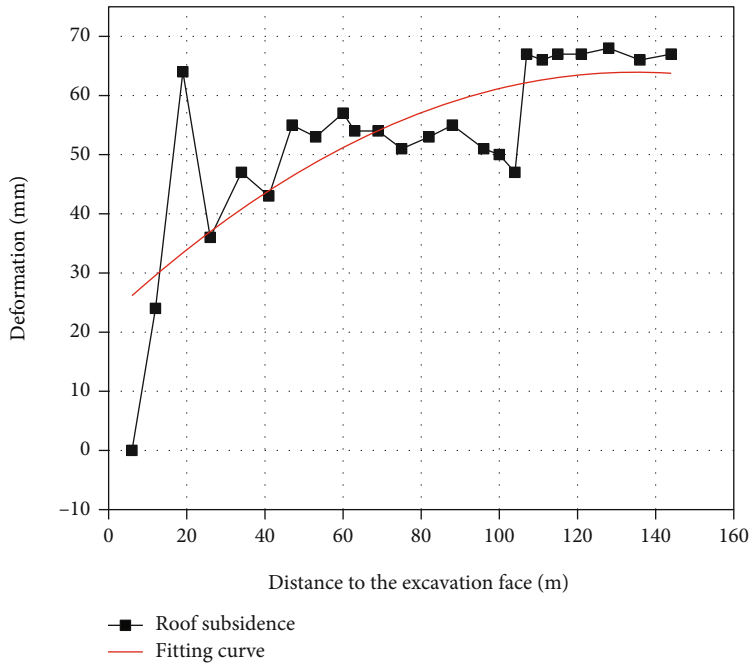


(c)

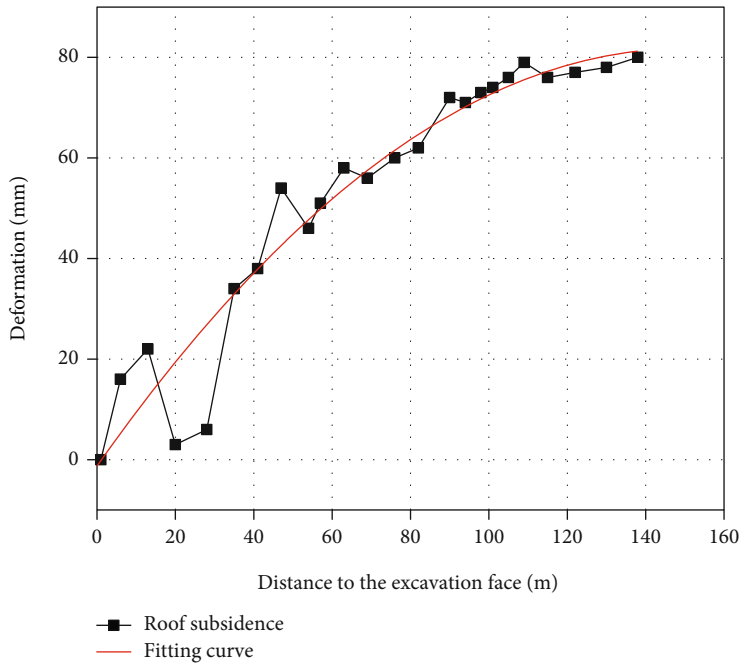


(d)

Figure 14: Continued.

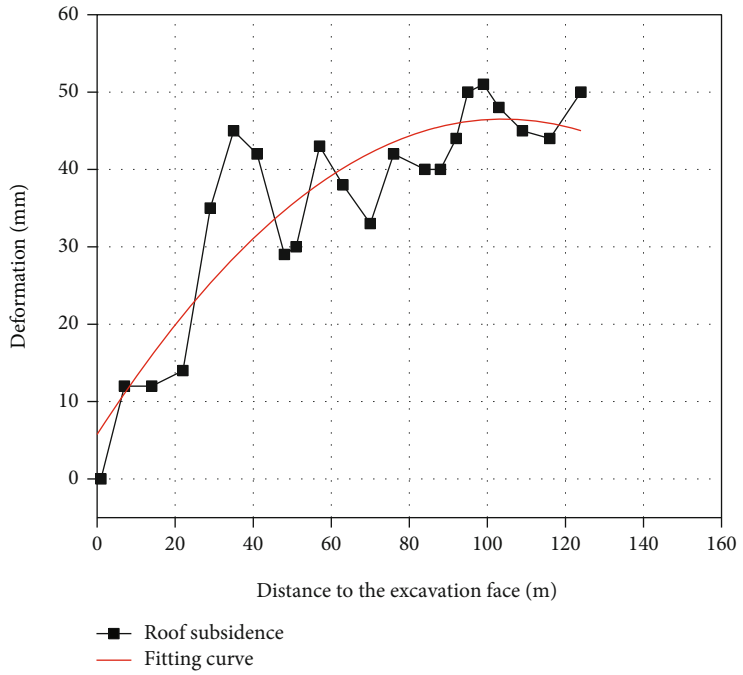


(e)

Figure 14: Monitoring results of roof subsidence.

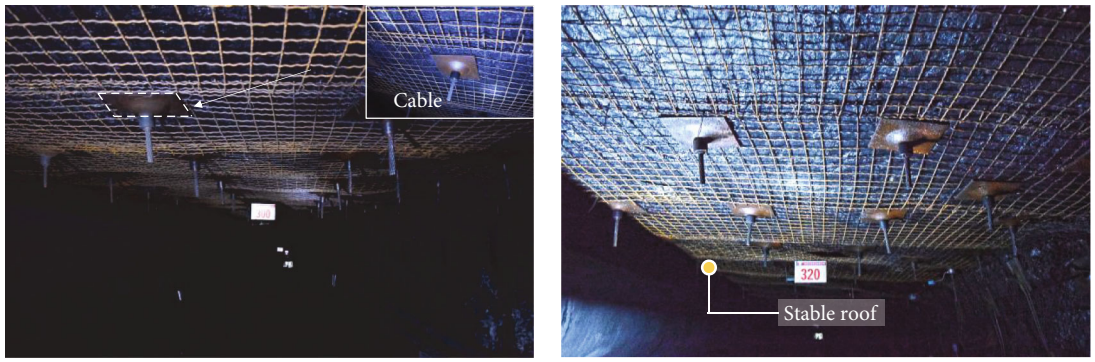


(a) (b)

Figure 15: Real photos of the roof under TADL support.

(3) The analysis of the deformation characteristics of station 3 is shown in Figure 14(c). After the excavation of the roadway space, the roof subsidence within the range of 0~34 m (0~7 d) undergoes severe deformation phase at speed greater than 10 mm/d. The range of 34~60 m (8~11 d) experienced slowing deformation phase, and the speed decreased from 10 mm/d to 2~4 mm/d. 60 m (12 d) after excavation, the stable deformation phase came into place at 0~1 mm/d. The subsidence from these three phases accounts for 70.1%, 14.9%, and 14.9% of the total, respectively. The maximum sinking speed of the roof is 12 mm/d, and the total sinking amount after the deformation is stable is 67 mm

(4) The analysis of the deformation characteristics of station 4 is shown in Figure 14(d). After the excavation of the roadway space, the roof subsidence within the range of 0~47 m (0~8 d) is in severe deformation at a speed greater than 10 mm/d; the subsidence in the severe deformation phase accounted for 67.5% of the total subsidence. The deformation slowed down in the range of 47~90 m (9-15 d), and the deformation speed decreased from 10 mm/d to 3~5 mm/d; the subsidence in the phase of slowing deformation accounted for 22.5% of the total subsidence. 90 m (16 d) after excavation entered the stable deformation phase, the deformation speed remained at 0~1 mm/d. The maximum subsidence rate of the roof is 28 mm/d, and the

total subsidence amount after the deformation is stable in 80 mm

(5) The analysis of the deformation characteristics of station 5 is shown in Figure 14(e). After the excavation of the roadway space, the roof subsidence within the range of 0~29 m (0~5 d) is in a phase of severe deformation at a speed greater than 7 mm/d. The deformation slowed down in the range of 29~57 m (6~10 d), with the average rate decreasing from 7 mm/d to 3~4 mm/d. 57 m (11 d) after excavation entered the stable deformation phase, with the deformation speed maintained at 0~1 mm/d. The subsidence from these three phases accounts for 70%, 16%, and 14% of the total, respectively. The maximum subsidence speed of the roof was 8 mm/d, and the total subsidence amount after the deformation stabilized was 50 mm

Besides, the fluctuation of the curve is caused by the error in the measurement process. In the field practice, we adopted the traditional cross-section measurement method for displacement monitoring. The measurement accuracy is affected by objective factors such as the wind speed at the roadway, the level and plumbness of the engineering line, and the level and plumbness of the tape measure.

Figure 15 is a photo of the headentry of $14^{-1}105$ using the TADL support illustrating the support effect. It can be seen from the figure that after using this technique, the roof coal body has a good forming effect, the surface is smooth, and the support members have no uneven deformation. This shows that the best time for surrounding rock control is the early stage of roadway excavation. At this time, the TADL support technique featuring high-preload and thick-layer anchoring is applied to the roof rock mass in an elastic state, which can effectively control the deformation of the surrounding rock.

## 6. Conclusions

In this paper, a thick-anchored dual-layer locking supporting technique is proposed. The mining conditions of gob-side entry with small coal pillars are selected for engineering application and verification. The conclusions are as follows:

(1) The numerical calculation results show that the TADL support technique can drive away the tensile stress, which is mainly related to high-preload and thick-layer anchoring. After roadway excavation, high-preload force active support is applied in the initial stage of stress release, which can avoid the tensile deformation and separation of the roof rock mass in the initial stage

(2) Numerical calculation results show that, compared with the original support scheme, the roof displacement of the roadway is significantly reduced by more than 16% after adopting the TADL support technique

(3) The results of on-site industrial experiments show that the initial stage of roadway excavation is the best period for stabilizing the surrounding rock. At this time, the TADL support technique featuring high-preload and thick-layer anchoring is applied to the roof rock mass in an elastic state, which can effectively control the deformation of the surrounding rock

## Data Availability

The data used to support the findings of this study are included within the article.

## Conflicts of Interest

The authors declare that they have no conflict of interest to this work.

## Acknowledgments

The work of this paper is financially supported by the Fundamental Research Funds for the Central Universities (2019QNA23).

## References

[1] J. B. Bai, W. L. Shen, G. L. Guo, X. Y. Wang, and Y. Yu, "Roof deformation, failure characteristics, and preventive techniques of gob-side entry driving heading adjacent to the advancing working face," *Rock Mechanics and Rock Engineering*, vol. 48, no. 6, pp. 2447–2458, 2015.

[2] Y. Wang, P. F. Tan, J. Han, and P. Li, "Energy-driven fracture and instability of deeply buried rock under triaxial alternative fatigue loads and multistage unloading conditions: prior fatigue damage effect," *International Journal of Fatigue*, vol. 168, article 107410, 2023.

[3] Y. Wang, Y. Su, Y. Xia, H. Wang, and X. Yi, "On the effect of confining pressure on fatigue failure of block-in-matrix soils exposed to multistage cyclic triaxial loads," *Fatigue & Fracture of Engineering Materials & Structures*, vol. 45, no. 9, pp. 2481–2498, 2022.

[4] Y. X. Yuan, C. L. Han, N. Zhang et al., "Zonal disintegration characteristics of roadway roof under strong mining conditions and mechanism of thick anchored and trans-boundary supporting," *Rock Mechanics and Rock Engineering*, vol. 55, no. 1, pp. 297–315, 2022.

[5] Y. Wang, T. Mao, Y. Xia, X. Li, and X. Yi, "Macro-meso fatigue failure of bimrocks with various block content subjected to multistage fatigue triaxial loads," *International Journal of Fatigue*, vol. 107014, 2022.

[6] Y. Wang, X. Yi, P. Li, M. Cai, and T. Sun, "Macro-meso damage cracking and volumetric dilatancy of fault block-in-matrix rocks induced by freeze–thaw-multistage constant amplitude cyclic (F-T-MSCAC) loads," *Fatigue & Fracture of Engineering Materials & Structures*, vol. 45, no. 10, pp. 2990–3008, 2022.

[7] R. Dehui, *The Rule of the Stope Pressure Distribution of Flat-Dipping Coal Bed and the Rational Arrangement of Workings*, China Coal Industry Publishing House, 1982.

[8] C. Hou and X. Li, "Stability principle of big and small structures of rock surrounding roadway driven along goaf in fully mechanized top coal caving face," *Journal of China Coal Society*, vol. 1, pp. 1–7, 2001.

[9] M. Qian, D. Zhang, L. Li, L. Kang, and J. Xu, "'S-R' stability for the Voussoir beam and its application," *Coal Technology Northeast China*, vol. 3, pp. 6–10, 1994.

[10] H. Xingzhu, L. Shu, L. Zenghui, C. Wenhua, and L. Yingfu, "Research on strata pressure characteristic of gob-side entry driving in island mining face and its engineering application," *Chinese Journal of Rock Mechanics and Engineering*, vol. 30, no. 8, pp. 1646–1651, 2011.

[11] L. Shiliang, "Analysis of the rock behaviour and the stress in surrounding rock of the roadway in pillarless mining," *Journal of China Coal Society*, vol. 4, pp. 29–37, 1981.

[12] Z. Nong, H. Changliang, and X. Zhengzheng, "Theory of continuous beam control and high efficiency supporting technology in coal roadway," *J. Min. Strat. Control Eng*, vol. 1, no. 2, article 013005, pp. 48–55, 2019.

[13] H. Changliang, Z. Nong, K. Jiaguang, and R. Zhi, "Mechanism and application of double active control with pressure-relieving and anchoring for gob-side entry retaining," *Journal of China Coal Society*, vol. 42, no. S2, pp. 323–330, 2017.

[14] Q. Wang, M. C. He, J. Yang, H. K. Gao, B. Jiang, and H. C. Yu, "Study of a no-pillar mining technique with automatically formed gob-side entry retaining for longwall mining in coal mines," *International Journal of Rock Mechanics and Mining Sciences*, vol. 110, pp. 1–8, 2018.

[15] M. He, C. Li, W. Gong, L. R. Sousa, and S. Li, "Dynamic tests for a constant-resistance-large-deformation bolt using a modified SHTB system," *Tunnelling and Underground Space Technology*, vol. 64, pp. 103–116, 2017.

[16] H. Wang, Y. Jiang, S. Xue et al., "Assessment of excavation damaged zone around roadways under dynamic pressure induced by an active mining process," *International Journal of Rock Mechanics and Mining Sciences*, vol. 77, pp. 265–277, 2015.

[17] H. Wang, R. Shi, C. Lu, Y. Jiang, D. Deng, and D. Zhang, "Investigation of sudden faults instability induced by coal mining," *Safety Science*, vol. 115, pp. 256–264, 2019.

[18] H. Wang, S. Xue, R. Shi, Y. Jiang, W. Gong, and L. Mao, "Investigation of fault displacement evolution during extraction in longwall panel in an underground coal mine," *Rock Mechanics and Rock Engineering*, vol. 53, no. 4, pp. 1809–1826, 2020.

[19] V. Renaud, C. Balland, and T. Verdel, "Numerical simulation and development of data inversion in borehole ultrasonic imaging," *Journal of Applied Geophysics*, vol. 73, no. 4, pp. 357–367, 2011.